Check for updates

THE AMERICAN SOCIETY OF MECHANICAL ENGINEERS
345 E. 47th St., New York, N.Y. 10017

97-GT-80

The Society shall not be responsible for statements or opinions advanced in papers or discussion at meetings of the Society or of its Divisions or Sections, or printed in its publications. Discussion is printed only if the paper is published in an ASME Journal. Authorization to photocopy material for internal or personal use under circumstance not falling within the fair use provisions of the Copyright Act is granted by ASME to libraries and other users registered with the Copyright Clearance Center (CCC) Transactional Reporting Service provided that the base fee of $0.30 per page is paid directly to the CCC, 27 Congress Street, Salem MA 01970. Requests for special permission or bulk reproduction should be addressed to the ASME Technical Publishing Department.

Copyright © 1997 by ASME All Rights Reserved Printed in U.S.A

COMPUTATION OF DISCRETE-HOLE FILM COOLING: A HYDRODYNAMIC STUDY

Mulugeta K. Berhe and Suhas V. Patankar
Department of Mechanical Engineering
University of Minnesota
111 Church Street SE
Minneapolis, MN 55455

BREAK

Downloaded from http://asmedigitalcollection.asme.org/GT/proceedings-pdf/GT1997/78705/V003T09A011/2410525/v003t09a011-97-gt-080.pdf by guest on 17 August 2022

ABSTRACT

Hydrodynamic plots are presented from a numerical study conducted on a three dimensional film cooling geometry that includes the main flow, injection hole, and the plenum. The fully elliptic Navier-Stokes equations were solved over a body fitted grid using the control volume method. Turbulence closure was achieved using the k-ε turbulence model. The results presented include contour plots of the resultant velocity at hole exit, as well as streamwise mean velocity and turbulence intensity contours at several cross-stream planes. Computations were performed for blowing ratios of 0.5 and 1.0, and a density ratio of 2. The injection hole was 12.7 mm in diameter, 3.5 diameters long, and inclined at 35^0 to the streamwise direction. Results obtained from this analysis are compared with the available experimental results. Whereas the overall agreement is good, important differences were found. Compared to the experimental jet, the computed jet showed (a) a larger vertical velocity at hole exit, (b) a smaller lateral spread in the downstream region, especially at low blowing ratios.

NOMENCLATURE

D	diameter of injection hole
DR	density ratio = ρ_j/ρ_∞
k	turbulent kinetic energy
L	length of injection hole
M	blowing ratio = $\rho_j U_j/\rho_\infty U_\infty$
T_j	coolant jet temperature at hole exit
T_∞	freestream temperature
Tu	turbulence intensity level = $\sqrt{k/1.5}/U_\infty$
u_x	velocity component in the streamwise direction
u_y	velocity component in the lateral direction
u_z	velocity component in the vertical direction
U_j	coolant jet average exit velocity
U_∞	mainstream gas inlet velocity
V	resultant velocity = $\sqrt{u_x^2+u_y^2+u_z^2}$
X	streamwise distance measured from hole leading edge
Y	lateral distance measured from hole centerline plane
Z	vertical distance measured from the test surface
α	injection angle of coolant jet
ε	dissipation rate of turbulent kinetic energy
η	local adiabatic film cooling effectiveness
μ_t	turbulent viscosity
ρ_j	density of coolant jet
ρ_∞	density of the freestream fluid

INTRODUCTION

In numerical modeling of discrete-hole film cooling, one of the issues that need to be addressed is the adequacy of the turbulence models that are commonly used in film cooling applications, especially the k-ε turbulence model. It is important to know the errors involved in these computations so that appropriate allowances are made in design applications. One limitation that is often attributed to the k-ε turbulence model is the inadequate lateral spreading of the jet in the relaxation region. Several papers have discussed this issue in connection with effectiveness studies. However, the varying assumptions and limitations built in each of these studies have made an accurate assessment of the problem difficult. For example, many of these studies used assumed velocity profiles at hole exit which can very well affect the penetration and spreading characteristics of the jet.

In this paper, the flow development of jet-in-crossflow is studied using results obtained from a numerical study conducted on a realistic, three dimensional film cooling geometry used in the experimental study of Pietrzyk (1989). The geometry considered includes the mainflow area, injection hole, and supply plenum. The plots examined include contour plots of resultant velocity at hole exit as well as contour plots of the streamwise mean velocity and turbulence intensity at several cross-stream planes. These plots are used to study the

Presented at the International Gas Turbine & Aeroengine Congress & Exhibition
Orlando, Florida — June 2–June 5, 1997

differences and similarities between the computed and measured flow profiles, and to explain the computed adiabatic effectiveness values reported in a companion paper by Berhe and Patankar (1996).

In the sections to follow, a brief literature review is first presented. This will be followed by a description of the present numerical study, detailing such things as the geometric and flow variables used, and the computational methodology adopted. In the results and discussion section, the numerical results will be presented and discussed against the experimental results.

LITERATURE REVIEW

One of the most recent experimental work on the hydrodynamics of film cooling was conducted by Pietrzyk (1989) of the University of Texas at Austin. In this work, the flow development over a single raw of holes was studied. Among other things, they presented velocity and turbulence intensity profiles at hole exit as well as several cross-stream planes, and discussed the effects of velocity ratio and density ratio on these profiles.

Leylek and Zerkle (1994) numerically modeled the film cooling arrangement used by Pietrzyk (1989). Using the k-ε turbulence model, they showed the jetting effect of the coolant fluid through the upstream wall of the injection hole. They also presented an overall discussion on the flow field development downstream of the injection hole. However, no actual comparisons (with experiments) were given for the velocity profiles at hole exit or downstream of it.

Berhe and Patankar (1996) studied a film cooling arrangement similar to that of Leylek and Zerkle (1994), and examined various combinations of film cooling variables, including hole and plenum effects. Using the k-ε turbulence model, they modeled the film cooling arrangements used by Kohli and Bogard (1995), and Sinha, et al. (1991). They reported computed adiabatic effectiveness values that compared favorably with those reported in these two papers.

In this paper, we will study the hydrodynamics of film cooling. The results presented and discussed include contour plots of the resultant velocity profiles at hole exit, as well as contour plots of streamwise mean velocity and turbulence intensity at several cross-stream planes. These plots are compared with the experimental results of Pietrzyk (1989). Important differences and similarities are noted in jet spreading and penetration characteristics.

DETAILS OF THE PRESENT COMPUTATION

In this section, we will first present the parameters used in this study. We will then discuss the computational methodology, discretization, initialization, boundary conditions, and convergence criteria used in these computations.

Computational Parameters

Computations were performed on the geometric set-up shown in Fig. 1. The flow and geometric variables used are given in Table 1. These parameters were chosen to match the film cooling arrangement used by Pietrzyk (1989).

Discretization and Solution Methodology

The domain shown in Fig. 1 was discretized into 98/15/68 cells in the X/Y/Z directions. The injection hole was discretized into 10/5/24 cells in the X/Y/Z directions. Such a grid size was chosen as a compromise between the numerical accuracy on the one hand, and the cost of computation on the other. To test for grid independence, both 25% and 50% finer grids were used. Whereas the 25% finer grid resulted in about 3% increase in centerline effectiveness, the 50% finer grid resulted in a variable increase in centerline effectiveness of 4% (far downstream) to 8% (very near the hole). The computational times needed for the two finer grids were, however, 200% and 350%, respectively, of the original grid CPU time. As far as the hydrodynamic plots are concerned, differences between the plots for finest and coarsest grids were mostly localized near the jet core and close to the injection hole. Elsewhere, the plots were nearly identical. The discussions presented in this paper could very well have been made with either set of these plots.

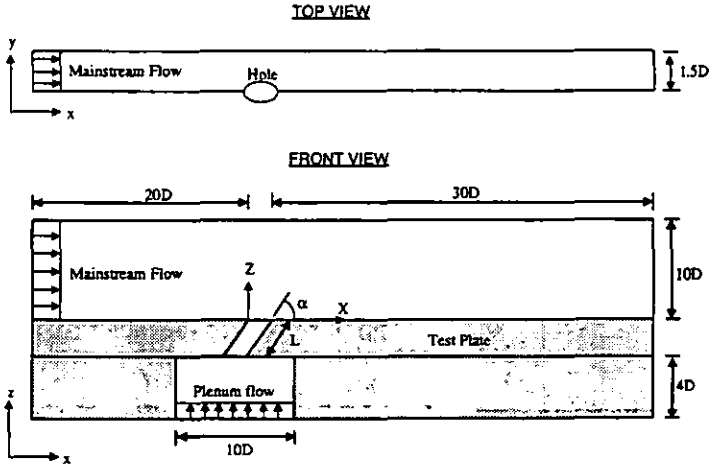

Fig. 1 The film cooling computational geometry

Table 1 Flow and geometric parameters

Variable	Value	Variable	value
U_∞	20 m/s	M	0.5, 1.0
T_∞	302 K	α	35°
Tu	0.2 %	L	3.5D
DR	2.0	D	12.7 mm

The near orthogonal grid system used inside the surface and volume elements of the above domains were generated by solving 2-D and 3-D Poisson equations, respectively. Grid stretching (or contraction) was limited to about 30%. The grid set-up in the vicinity of the injection hole is shown in Fig. 2.

The fully elliptic, three dimensional Navier-Stokes equations were solved over a single block body fitted grid using the control volume methodology described in Patankar (1980).

Downloaded from http://asmedigitalcollection.asme.org/GT/proceedings-pdf/GT1997/78705/V003T09A011/2410525/v003t09a011-97-gt-080.pdf by guest on 17 August 2022

Turbulence closure was achieved using the standard k-ε model and the wall function approach described in Launder and Spalding (1974). Discretization was controlled to achieve z+ (or x+) values of about 50, 30 and 20 inside the main flow, film hole, and the plenum, respectively.

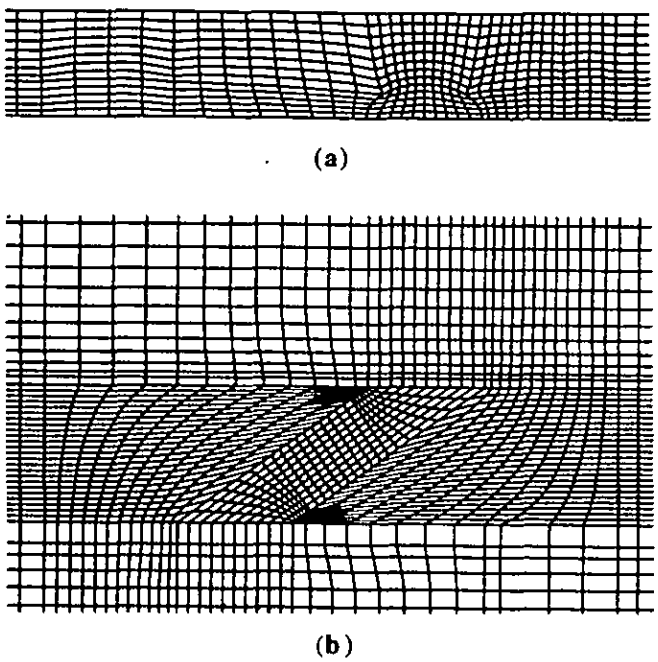

(a)

(b)

Fig. 2 A partial view of the grid in the vicinity of the hole. (a) xy view at hole exit, (b) xz view in the centerline plane

Initialization

As has been found by previous investigators, a good initialization as well as proper relaxation factors were found critical for the convergence behavior of these computations, especially when the blowing ratio is high. In these computations, a relaxation factor of 0.6 was used for the three velocity components and the temperature, and 0.4 was used for the k, ε and μ_t. Pressure was not relaxed.

For a blowing ratio of 0.5, domain initialization was done as follows. In the interior of the domain, k and ε were initialized using the following formulas.

$$k = 1.5T_u^2U_\infty^2 \qquad (1)$$

$$\varepsilon = \frac{20C_\mu^{3/4}k^{3/2}}{D} \qquad (2)$$

A high turbulence level of about 20% was assumed everywhere in the domain, except at inlet. At inlet, the desired freestream turbulence of 0.2% was imposed. In the main flow, the streamwise velocity and temperature were assigned their respective freestream values everywhere. The lateral and vertical velocities were made zero. In the plenum and injection hole, constant axial velocities were assigned depending on the blowing ratio and the local flow area under consideration. In these two regions, the temperature was assigned a constant value equal to the prescribed coolant temperature.

For a blowing ratio of 1.0, the domain was initialized using a converged solution for M=0.5. The velocity field was initialized by appropriately scaling the velocity field for M=0.5 to reflect the change in blowing ratio. Such a scaling of the velocity field in the affected area (main area or plenum) was found essential for good convergence. Thus, unlike in some of the previous numerical studies, Leylek and Zerkle (1994), for example, the expensive routine of marching to higher blowing ratios using small increments of the blowing ratio was avoided in these computations.

Boundary Conditions

Symmetry conditions were imposed on the two bounding lateral planes. At the top plane in the mainstream, both zero flux and zero vertical velocity conditions were imposed. At the outflow boundary, zero gradient condition was imposed for all the variables.

Convergence Criteria

Both the normalized residuals and the change in cooling effectiveness values were monitored to establish convergence. Computations were assumed converged when the normalized residuals were of the order of 1e-4. In a typical computation at a blowing ratio of 0.5, a good convergence was achieved in about 350 iterations. One iteration took about 30 seconds of CPU time in a 9 processor, CRAY C916/9512 Supercomputer. For a blowing ratio of 1.0, convergence was achieved in about 250 iterations, starting from a converged solution for M=0.5.

RESULTS AND DISCUSSION

The results presented and discussed in this section are contour plots of the resultant velocity at hole exit, as well as contour plots of the streamwise mean velocity and turbulence intensity at several cross-stream planes. The turbulence intensity at hole exit is not shown here because no corresponding experimental data is available.

The Velocity Field at Hole Exit

Figures 3a and 3b show the numerical and experimental velocity distributions at hole exit, respectively, for a blowing ratio of 0.5. The velocity plotted in both of these figures is the resultant velocity, V, and was taken at 0.05D distance above the hole exit.

In both of these figures, the velocity distribution through much of the exit area is around $0.4U_\infty$, and increases to $0.5U_\infty$ near the trailing edge of the injection hole. Examination of the individual velocity components shows that whereas the dominant velocity is the streamwise velocity, the lateral velocity is negligibly small ($\sim 0.05U_\infty$). Furthermore, the computed vertical velocity was found larger than the experimentally found vertical velocity, indicating a larger penetration of the computed jet. The computed vertical velocity varied from 0 at the leading edge to $0.4U_\infty$ at the trailing edge, as opposed to a vertical velocity variation of 0 to $0.2U_\infty$ for the experimental jet.

Downloaded from http://asmedigitalcollection.asme.org/GT/proceedings-pdf/GT1997/78705/V003T09A011/2410525/v003t09a011-97-gt-080.pdf by guest on 17 August 2022

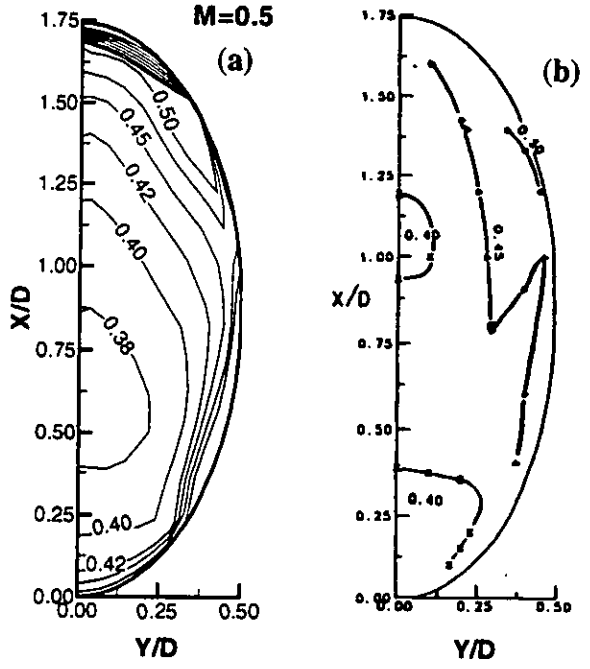

Fig. 3 Normalized resultant velocity (V/U_∞) at hole exit, M=0.5 (a) Numerical result, (b) Experimental result of Pietrzyk (1989)

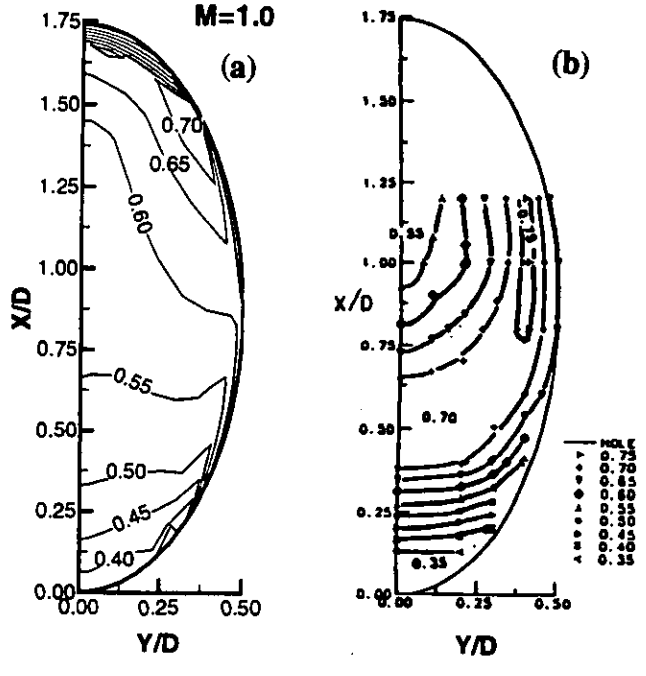

Fig. 4 Normalized resultant velocity (V/U_∞) at hole exit, M=1.0 (a) Numerical result, (b) Experimental result of Pietrzyk (1989)

Figures 4a and 4b show the numerical and experimental resultant velocity distributions at hole exit, respectively, for a blowing ratio of 1. As can be seen from these plots, there is a difference between the velocity distributions in these two figures. In the numerical plot, the exit velocity progressively increases from $0.4U_\infty$ near the leading edge, to $0.7U_\infty$ near the trailing edge of the hole. In the experimental plot, on the other hand, the exit velocity starts at $0.35U_\infty$ near the leading edge, and quickly reaches $0.7U_\infty$ at X/D=0.5, and then decreases. Near X/D=1, the numerical plot shows a nearly uniform velocity distribution of $0.6U_\infty$. At this location, the experimental plot shows a velocity distribution which is laterally varying from $0.55U_\infty$ to $0.75U_\infty$. No measured data is available at the trailing edge of the hole.

Again, examination of the individual velocity components shows that the dominant velocity is the streamwise velocity, and that the lateral velocity is small ($<0.1U_\infty$). Furthermore, the computed vertical velocity was found about 20% larger than the one found experimentally, indicating a larger penetration of the numerical jet into the freestream.

The Streamwise Mean Velocity Field

Figures 5 and 6 show the numerical and experimental streamwise mean velocity contour plots, respectively, for a blowing ratio of 0.5. Four contour plots are shown in each of these figures corresponding to streamwise locations of 1D, 5D, 10D, and 15D from the leading edge of the hole. From these plots, we may note that:

1. Compared to the experimental plots, the numerical plots show more jet penetration into the freestream accompanied by a less spread in the lateral direction. The u_X/U_∞=0.95 contour line in the numerical plots is, on the average, 0.25D further away from the wall in the centerline plane, and 0.20D nearer to the wall in the mid-pitch plane. The less lateral spread evident in the numerical results explains the relatively poorer prediction of the laterally averaged effectiveness at M=0.5 reported in Berhe and Patankar (1996).

2. The location of the core of the jet is about the same in both the experimental and numerical plots. This explains the relatively good agreement found between the computed and experimental centerline effectiveness results reported in Berhe and Patankar (1996).

3. The relaxation of the flow field downstream of the injection hole is comparable in both cases. Between X/D=I and X/D 15, the boundary layer in both cases grew a vertical distance of about 0.65D at the centerline plane, and 0.15D in the mid-pitch plane. This trend continued all the way to the outflow boundary located at X/D=30.

Figures 7 and 8 show a side by side comparison of the numerical and experimental streamwise mean velocity contour plots, respectively, for a blowing ratio of 1.0. The four plots in each figure are for X/D locations of 1, 5, 10, and 15. From these plots, we may again note that:

1. Near the centerline plane, the numerical plots show a greater jet penetration into the freestream than is shown in the experimental plots. However, unlike in the previous results for

Downloaded from http://asmedigitalcollection.asme.org/GT/proceedings-pdf/GT1997/78705/V003T09A011/2410525/v003t09a011-97-gt-080.pdf by guest on 17 August 2022

M=0.5, the height of the boundary layer in the mid-pitch plane in both the numerical and experimental plots is about the same. The maximum difference is within 0.1D. This probably explains the better prediction of the laterally averaged effectiveness at M=1 reported in Berhe and Patankar (1996).

2. Both the numerical and experimental results indicate some jet lift-off, as shown by the closed contour lines near the jet core at X/D=5. As discussed in connection with Figures 4a and 4b, and evident in Figures 7 and 8, the computed jet has, however, a larger penetration than the experimental one.

3. The relaxation behavior of the two flow fields is slightly different. Between X/D=1 and X/D=15, the boundary layer at the centerline plane grew a vertical distance of 0.75D in the experimental plot, compared to 0.9D in the numerical plot. In the mid-pitch plane, on the other hand, both flow fields show little growth until X/D=15. Beyond that, the experimental plot showed more relaxation than the numerical plot.

The Turbulence Intensity Field

Figures 9 and 10 show the numerical and experimental turbulence intensity contour plots, respectively, for a blowing ratio of 0.5. These plots are for X/D locations of 1, 5, 10, and 15. From these figures, we may observe that:

1. The shapes of the corresponding contour lines in the two figures are very comparable.

2. As was the case with the streamwise mean velocity contour plots, some differences exists between the vertical locations of corresponding contour lines in the two figures. In the centerline plane, the computed contour lines are located 0.05D to 0.2D higher than the corresponding experimental contour lines. In the mid-pitch plane, on the other hand, the computed contour lines are located 0.1D to 0.2D lower than the corresponding experimental contour lines. This is simply a reflection of the streamwise mean velocity contour plots discussed earlier.

Figures 11 and 12 show the numerical and experimental lateral plane turbulence intensity contour plots, respectively, for M=1. These plots display characteristics similar to the plots for M=0.5. However, we may additionally note that:

1. Both the computed and measured turbulence levels at M=1 are slightly lower than those found at M=0.5, especially in the near-field region. This is due to the greater velocity difference between the jet and freestream at M=0.5, and simply confirms the shear layer between jet and freestream as the main source of turbulence.

2. At X/D=1 and immediately above the hole, the experimental plot shows a higher turbulence level than is shown in the corresponding numerical plot. This is probably a reflection of the higher lateral velocity gradient shown in Fig. 4b at this location.

CONCLUSIONS

In this paper, velocity and turbulence contour plots have been presented from a three dimensional film cooling computations. The film cooling arrangement considered includes the main flow, injection hole, and the plenum. The fully elliptic Navier-Stokes equations were solved over a body fitted grid using the control volume methodology. Turbulence closure was achieved using the standard k-ε model.

For the most part, the agreement between the predicted and measured velocity and turbulence profiles was good. Important differences were, however, noted between the computed and measured flow profiles. Differences were found in (a) velocity profiles at hole exit, (b) jet spreading characteristics following the injection hole.

For the blowing ratios of 0.5 and 1.0 considered, the computed jet exhibited a larger vertical velocity at hole exit than was found experimentally, especially near the trailing edge. This resulted in a deeper penetration of the numerical jet. Moreover, compared to the experimental jet, the computed jet showed less spread in the lateral direction and more spread in the vertical direction. The inadequate lateral spread of the computed jet was found more serious at the lower blowing ratio than at the higher one.

Future work may thus address not only the spreading characteristic of the jet following the injection hole, but also the velocity distribution within the hole itself.

ACKNOWLEDGEMENTS

The first author gratefully acknowledges the Doctoral Fellowship he received from the Natural Sciences and Engineering Research Council of Canada. Also, the financial grant of NASA Lewis Research Center, the computing facility of the Minnesota Supercomputer Institute, and the many useful suggestions of Dr. Kailash Karki of Innovative Research Incorporated are greatly appreciated.

REFERENCES

Berhe, M. K. and Patankar, S. V., 1996, "A Numerical Study of Discrete-Hole Film Cooling," ASME IMECE, Atlanta, GA.

Kohli, A., and Bogard, D. G., 1995, "Adiabatic Effectiveness, Thermal Fields, and Velocity Fields for Film Cooling with Large Angle Injection", ASME Paper 95-GT-219.

Launder, B. E., and Spalding, D. B., 1974, "The Numerical Computation of Turbulent Flows", *Computer Methods in Applied mechanics and Engineering*, Vol. 3, pp. 269-289.

Leylek, J. H., and Zerkle, R. D., 1994, "Discrete-Jet Film Cooling: A Comparison of Computational Results with Experiments", *ASME Journal of Turbomachinery*, Vol. 116, pp 358-368.

Patankar, S. V., 1980, *"Numerical Heat Transfer and Fluid Flow"*, Hemisphere Publishing Corporation, New York, New York.

Pietrzyk, J. R., 1989, "Experimental Study of the Interaction of Dense Jets with a Crossflow for Gas Turbine Applications", Ph.D. Dissertation, University of Texas at Austin.

Sinha, A. K., Bogard, D. G., and Crawford, M. E., 1991, "Film Cooling Effectiveness of a Single Row of Holes with Variable Density Ratio", *ASME Journal of Turbomachinery*, Vol. 113, pp 442-449.

Downloaded from http://asmedigitalcollection.asme.org/GT/proceedings-pdf/GT1997/78705/V003T09A011/2410525/v003t09a011-97-gt-080.pdf by guest on 17 August 2022

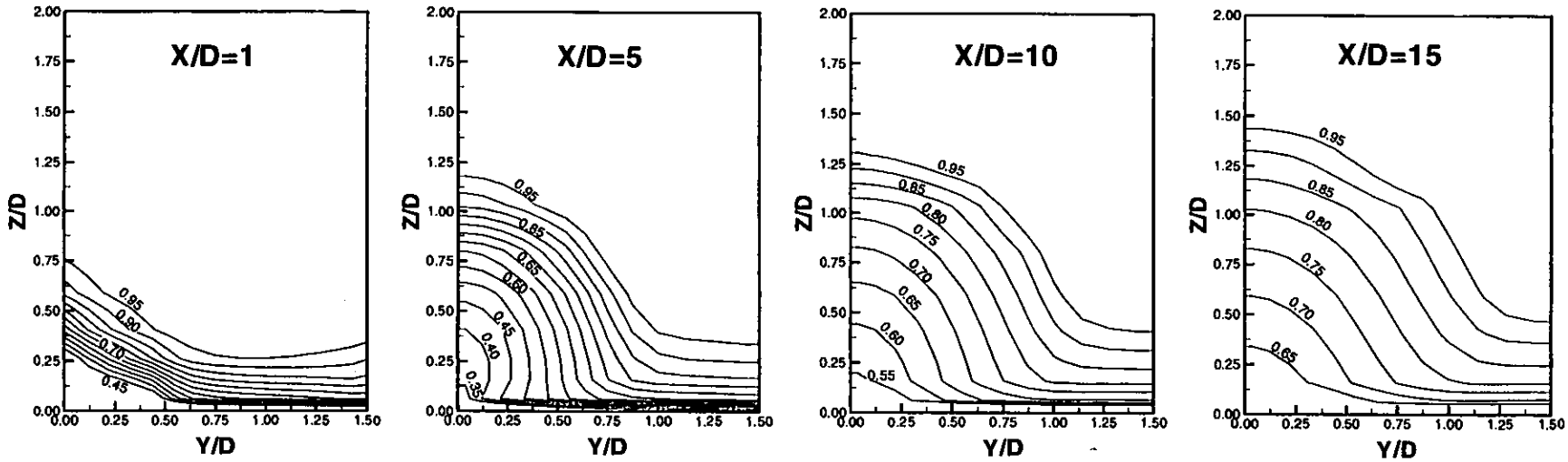

Fig. 5 Computed streamwise mean velocity contour plots at four cross-stream planes, M=0.5.

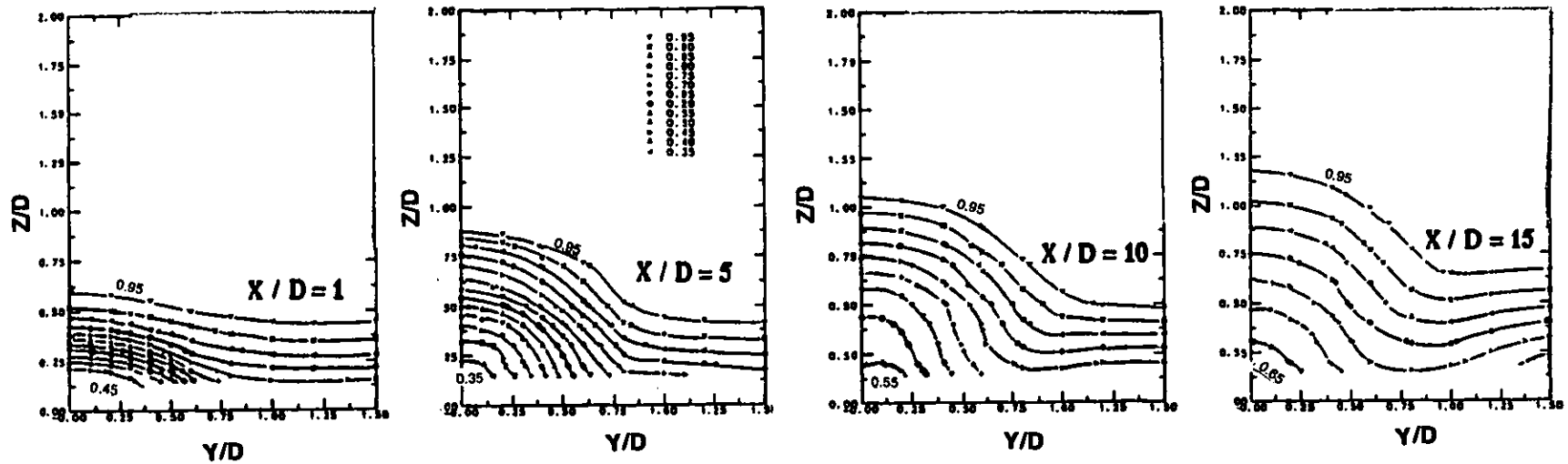

Fig. 6 Experimental streamwise mean velocity contour plots at four cross-stream planes, M=0.5, Pietrzyk (1989).

Downloaded from http://asmedigitalcollection.asme.org/GT/proceedings-pdf/GT1997/78705/V003T09A011/2410525/v003t09a011-97-gt-080.pdf by guest on 17 August 2022

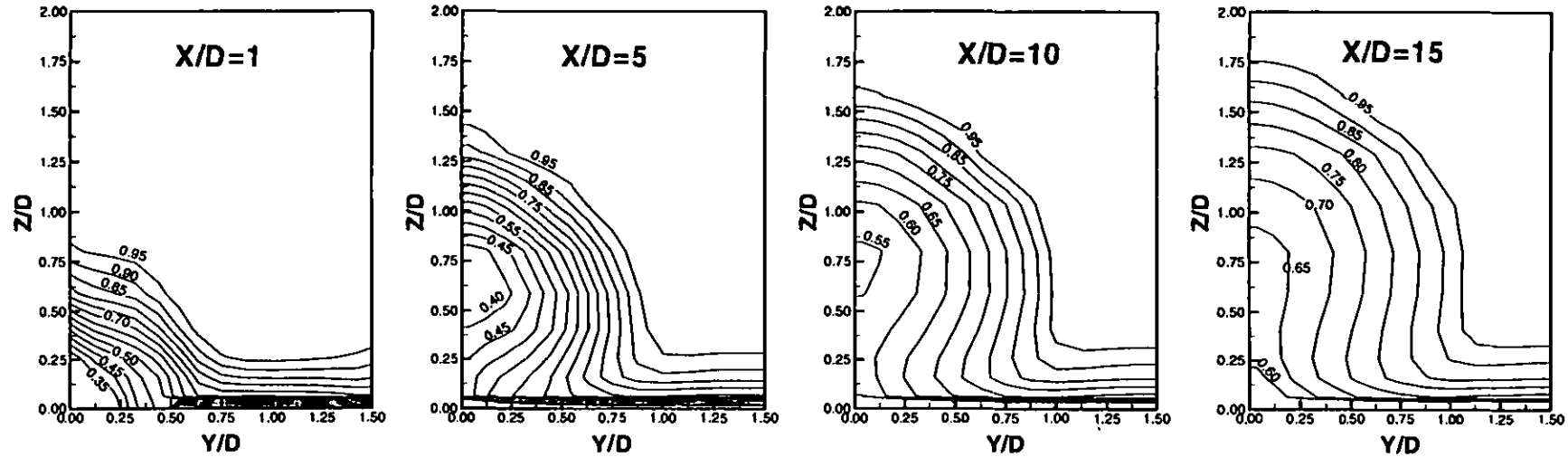

Fig. 7 Computed streamwise mean velocity contour plots at four cross-stream planes, M=1.0.

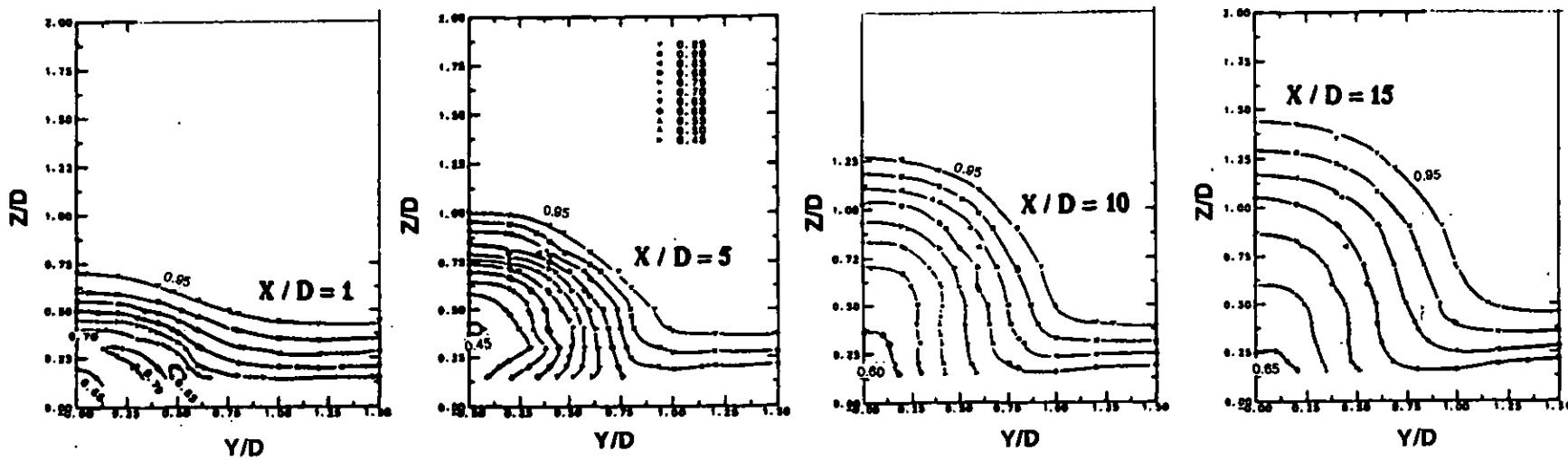

Fig. 8 Experimental streamwise mean velocity contour plots at four cross-stream planes, M=1.0, Pietrzyk (1989).

Downloaded from http://asmedigitalcollection.asme.org/GT/proceedings-pdf/GT1997/78705/V003T09A011/2410525/v003t09a011-97-gt-080.pdf by guest on 17 August 2022

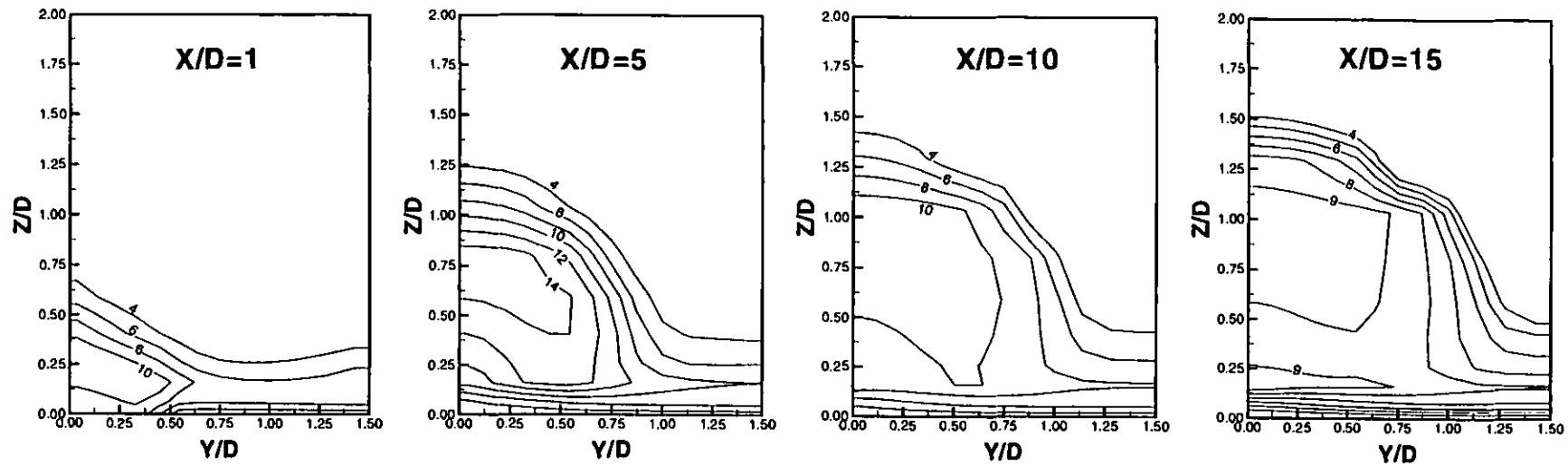

Fig. 9 Computed turbulence intensity contour plots at four cross-stream planes, M=0.5.

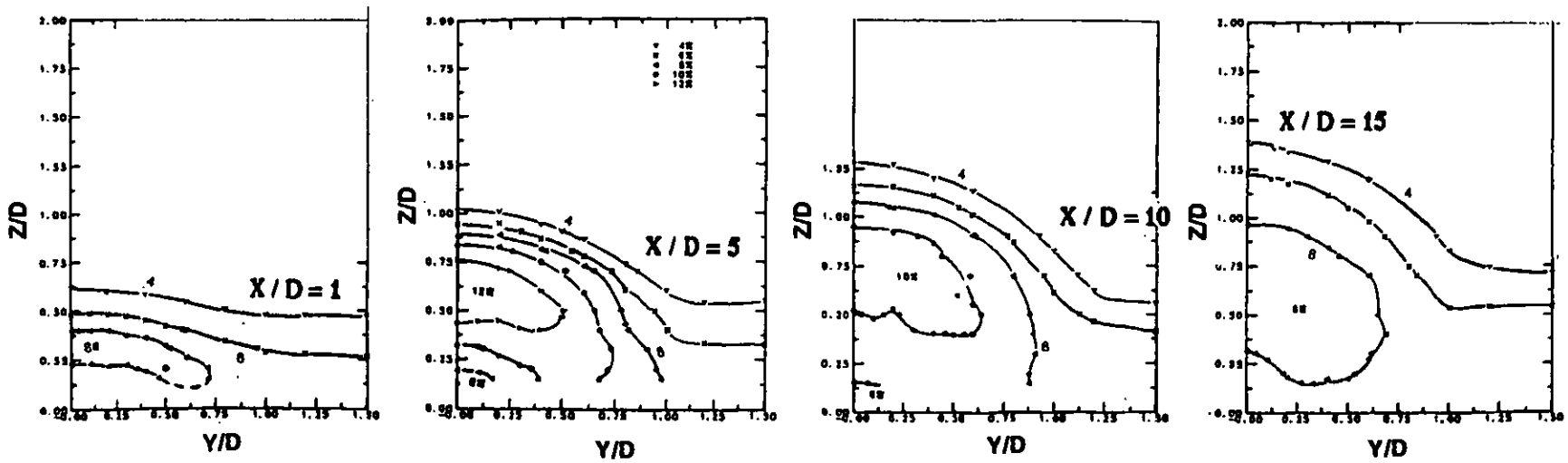

Fig. 10 Experimental turbulence intensity contour plots at four cross-stream planes, M=0.5, Pietrzyk (1989).

Downloaded from http://asmedigitalcollection.asme.org/GT/proceedings-pdf/GT1997/78705/V003T09A011/2410525/v003t09a011-97-gt-080.pdf by guest on 17 August 2022

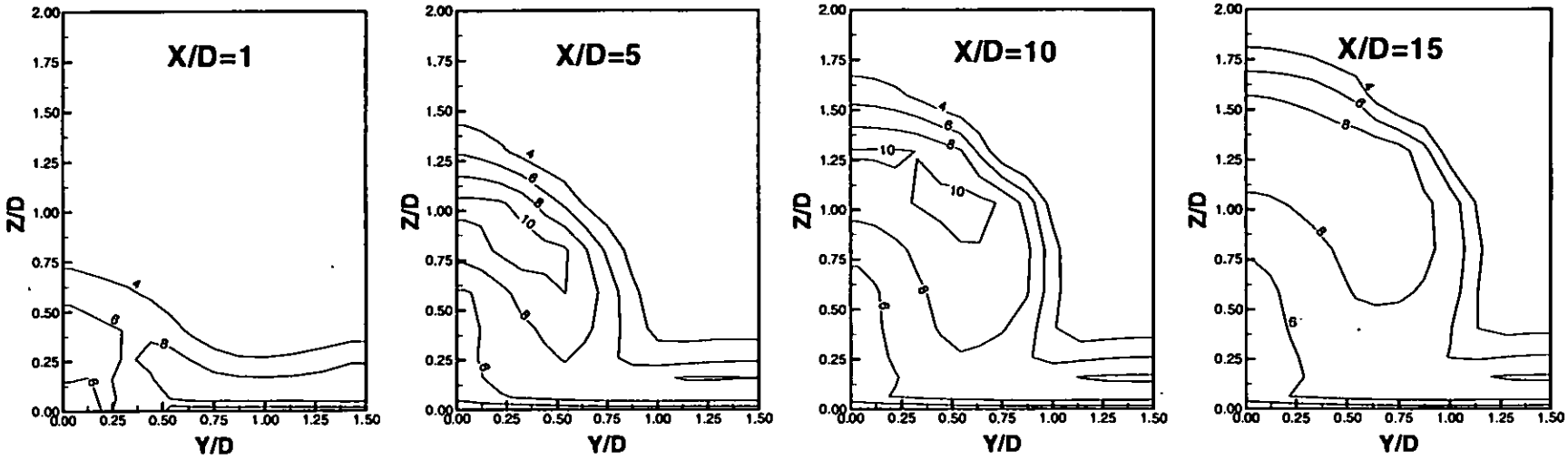

Fig. 11 Computed turbulence intensity contour plots at four cross-stream planes, M=1.0.

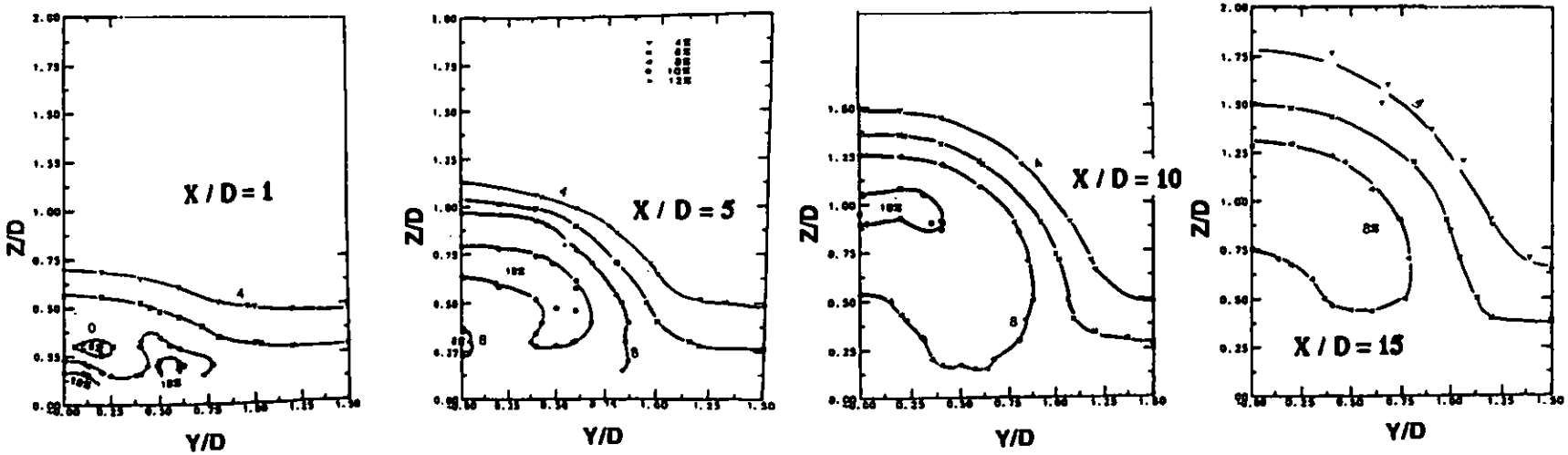

Fig. 12 Experimental turbulence intensity contour plots at four cross-stream planes, M=1.0, Pietrzyk (1989).

Downloaded from http://asmedigitalcollection.asme.org/GT/proceedings-pdf/GT1997/78705/V003T09A011/2410525/v003t09a011-97-gt-080.pdf by guest on 17 August 2022